The phase diagram and morphology of blends of poly(vinylidene fluoride) and poly(ethyl acrylate)

Robert M. Briber and F. Khoury
Polymers Division, National Bureau of Standards, Gaithersburg, MD 20899, USA
(Received 13 March 1986)

The phase diagram and crystallization behaviour of the polymer blend system consisting of poly(vinylidene fluoride) (PVF_2) and poly(ethyl acrylate) (PEA) have been examined. The melt exhibits phase separation upon heating to 10°C–50°C above the melting point of the PVF_2, depending on the composition. The cloud point and equilibrium melting point curve (for α-PVF_2) intersect at about 180°C and a composition of 50% (by weight) PVF_2. The polymer–polymer interaction parameter, χ, was calculated from the equilibrium melting point depression data and found to be -0.16 (at 170°C). Spherulite growth rate data have been measured as a function of composition and temperature. Assuming regime II crystallization a value of the product of the surface free energies of the α-PVF_2 crystals was calculated to be 4.4×10^{-4} J^2 m^{-4}. In blends crystallized from the one phase melt the texture of spherulites becomes more open and the spherulite extinction ring spacing (due to lamaller twist) becomes larger with increasing crystallization temperature. In addition the ring spacing increases with PEA content at constant crystallization temperature.

(Keywords: morphology; poly(vinylidene fluoride); poly(ethylene acrylate); phase diagram; polymer blends)

INTRODUCTION

Polymer blends have become increasingly more important as the need for polymeric materials with wider ranging properties has developed. While initial emphasis was on finding polymer pairs that were fully compatible it is now realized that systems exhibiting partial or even incomplete miscibility can have useful properties[1]. In the past, the majority of the work in the area of polymer miscibility has been on blends consisting of two non-crystallizable components while systems containing one (or two) crystallizable components have received much less attention[1,2]. The overall goal of the present study was to carefully establish the phase diagram of a blend system containing two polymers and which exhibits partial miscibility, phase separation and crystallization. Included in the objectives was an examination of the crystallization kinectics and morphology of the crystallizable component of the blend.

Probably the most widely studied crystallizable polymer with respect to its compatibility and properties in various polymer blends is poly(vinylidene fluoride) (PVF_2). Prior to the inception of the present study PVF_2 had been reported to be partially compatible with poly(vinyl acetate)[3], poly(methyl methacrylate) (PMMA)[4,5], poly(ethyl methacrylate)[6], poly(vinyl methyl ketone)[7] and poly(ethyl acrylate)[8]. It is generally accepted that the high degree of miscibility of PVF_2 with these polymers is due to a specific interaction between the dipole moment in PVF_2 and the carbonyl oxygen in the other polymers[7].

In the present paper we report the results of a determination of the phase diagram of the PVF_2/PEA blend system, and an examination of the crystallization kinetics as well as aspects of the morphology of the PVF_2 (in the α-crystalline form[9]) in these blends. Blends of these polymers had previously been briefly studied by Wahrmund *et al.*[8] who reported that they were partially miscible and were compatible in the liquid state at compositions having $\geqslant 30\%$ PEA. Much more recently, Enders *et al.*[10] have also investigated the PVF_2/PEA phase diagram. The cloud points determined in the present study agree closely with those of Enders *et al.* for blends containing 55% PVF_2 or less.

A lower critical solution temperature (*LCST*) is a well established phenomenon in polymer mixtures. The phase behaviour is as shown in *Figure 1a*. In a compatible blend system containing one crystalline component B), the melting point of the crystallizable polymer will be depressed due to the decrease in the chemical potential of that component in the mixture relative to the pure liquid. A schematic phase diagram for such a system is shown in *Figure 1b*. Nishi and Wang, using the Flory–Huggins expression for the free energy of mixing, have shown that one can obtain the polymer–polymer interaction parameter, χ, from an analysis of the melting point depression[5,11].

If the melting point curve and liquid–liquid phase separation curve intersect then the phase diagram becomes more complex as shown in *Figure 1c*. While understanding of the basic structure of such a phase diagram (as presented in *Figure 1c*) is a necessity for understanding the phase separation and crystallization behaviour in a partially compatible blend containing a crystallizable polymer, it has generally not been discussed in detail in the literature. The free energy curves for various temperatures indicated on the phase diagram are shown in *Figures 1d–g*. At T_1 (see *Figure 1d*), below the melting point, the crystals are in equilibrium with a liquid of mixed composition (l_1), except at very low B content

0032-3861/87/010038-09$3.00

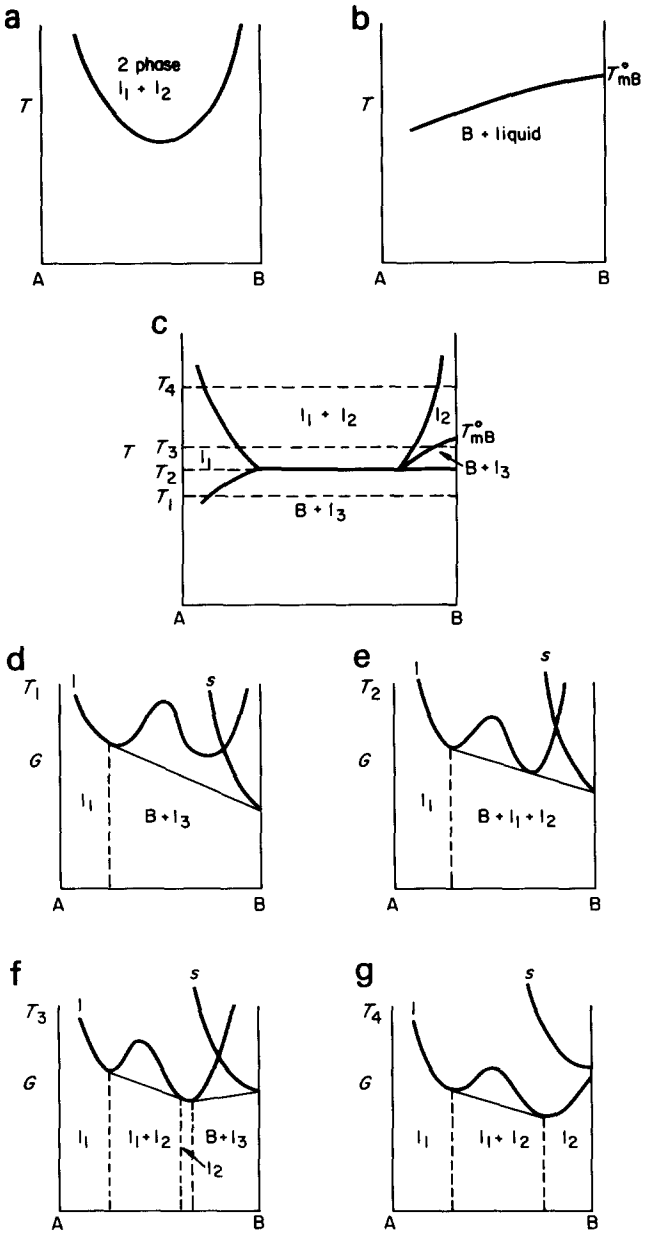

Figure 1 (a) Schematic phase diagram for a two component polymer blend exhibiting *LCST* behaviour; (b) schematic phase diagram for a two component polymer blend system with one crystalline component exhibiting a melting point depression; (c) phase diagram resulting from the overlap of (a) and (b); (d)–(g) free energy *versus* composition curves for the four temperatures indicated on (c); (d) T_1; (e) T_2; (f) T_3; (g) T_4

where the system is still above the melting point of the B (crystalline) component and is a one phase melt. At T_2 (see *Figure 1e*) the melting point curve and the phase separation curve intersect yielding a single temperature at which the B crystals are in equilibrium with two liquids l_1 and l_2. At low B content the melting point falls below T_2 and the system is a single phase liquid. At T_3 (see *Figure 1f*) there are four different regions in the phase diagram depending on composition. At low B content the system is a one phase melt. At intermediate compositions there are two liquids in equilibrium (above the *LCST*). At higher B content the system once again becomes a one phase liquid, while at the highest concentration of B the melting point is above T_3 and the system has B crystals in equilibrium with liquid. At T_4 (see *Figure 1g*) the temperature is everywhere above the melting point of the B component and the system exhibits a large region of two phase liquid behaviour at intermediate compositions and a one phase liquid region at the composition extremes.

EXPERIMENTAL

Polymers

The PVF_2 was obtained from Soltex Corporation[12] (XP8N resin) with $M_n = 47\,000$ and $M_w/M_n = 2.7$ (as measured by g.p.c. by the manufacturer). The PEA was purchased from Scientific Polymer Products, Inc.[12] and had a number average molecular weight of 29 000 and $M_w/M_n = 2.4$ as determined by g.p.c. The polymers were blended by dissolving them in the desired weight ratio in dimethyl formamide (DMF) at a concentration of about 10–20% polymer by weight. The solution was thoroughly mixed and then the polymers were precipitated by pouring into distilled water. All composition ratios referred to subsequently in the paper are given on a weight basis.

Cloud point measurements

Based on the early work of Paul *et al.*[8] the PVF_2/PEA blend system was expected to show miscibility at low PVF_2 content (with phase separation on heating) and incompatibility at high PVF_2 content. In order to measure the cloud point curve a photodiode was mounted in place of the eyepiece of an optical microscope to measure changes in the turbidity of the sample as it was heated in a Mettler FP-2 hot stage[12]. The photodiode output was fed to a chart recorder and the onset of the increase in turbidity was taken as the cloud point. Cloud points were measured at 10, 2 and 0.2°C/min. The faster heating rates allowed the approximate location of the cloud point to be determined before scanning at 0.2°C/min. The values measured at 0.2°C/min were taken as the cloud point and are given as a function of composition in *Table 1*. The cloud point curve is usually taken as an approximation to the binodal though this is only valid at slow heating rates. Cloud points were measured from a composition of 5/95 PVF_2/PEA (weight ratio) to 55/45 PVF_2/PEA. At 60% PVF_2 content and higher, it was not possible to measure the cloud point temperatures and the system exhibited two phase behaviour in the melt. Although there should be a single phase region at the PVF_2 rich side of the phase diagram, none was observed up to a composition of 95/5 PVF_2/PEA.

Table 1 Cloud points and T_m° values as a function of composition

Composition PVF_2/PEA by weight	Cloud point °C (0.2°C/min)	T_m° (°C)
10/90	229	174
15/85	225	
20/80	220	178
25/75	212	
30/70	208	180
35/65	201	
40/60	194	181
45/55	188	
50/50	181	182
55/45	173	
60/40	–	178
80/20	–	180
100	–	184

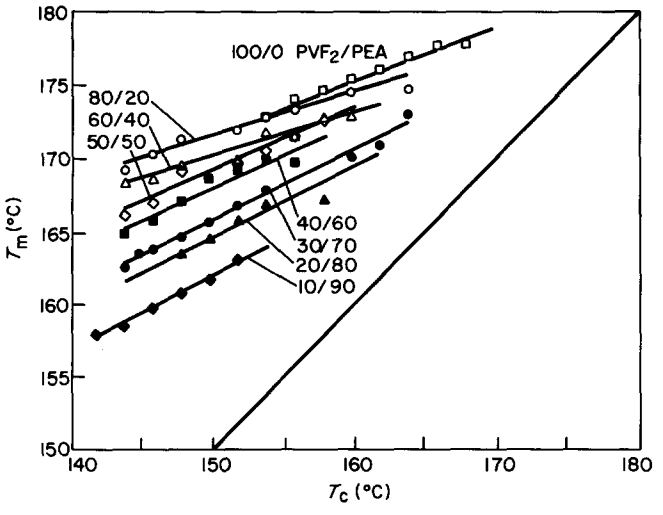

Figure 2 Plot of T_m *versus* T_c used to determine T_m° for the different blend compositions

Differential scanning calorimetry

Melting points were measured using differential scanning calorimetry (d.s.c.) on a series of isothermally crystallized samples as a function of composition and crystallization temperature (T_c). In general the scan rate used was 20°C/min. The effects of recrystallization and superheating were established not to be significant with respect to the melting point measured at 20°C/min by performing exploratory experiments at other heating rates. The melting temperatures for the various samples were taken as the maximum in the endothermic peak associated with the various crystal forms. The peak maximum was chosen because of the complicated nature of d.s.c. traces for PVF_2 crystallized at high temperatures due to the presence of both the alpha and gamma[9] crystal forms[11].

Only the alpha crystal form (as determined from melting points and electron diffraction[13]) of PVF_2 was observed at all crystallization temperatures except the highest (>155°C) where a small amount of the gamma structure also occurred. In all the subsequent experimental work presented in this paper only the alpha form of PVF_2 will be discussed.

Optical microscopy

Spherulite growth rates were measured by photographing the spherulites as a function of time at various crystallization temperatures in an optical microscope. The initial radial growth of spherulites increased linearly with time in all cases. At high crystallization temperatures, where growth is relatively slow, the spherulites stopped growing before impingement due to depletion of the PVF_2 and the growth deviated from linearity at the later stages of crystallization.

RESULTS AND DISCUSSION

The PVF_2 melting points as measured by d.s.c. are plotted *versus* crystallization temperature (Hoffman–Weeks plot[14]) in *Figure 2* and extrapolated to the line where $T_m = T_c$ to obtain the equilibrium melting point, T_m°. The equilibrium melting points for α-PVF_2 as a function of composition are given in *Table 1* (with the corresponding cloud points). The equilibrium melting temperature for the PVF_2 examined in this work is lower than the value obtained by Morra and Stein (184°C *versus* 201°C)[11], but they pointed out the extrapolated equilibrium melting point appears to depend on the head-to-head defect content of the polymer. Morra and Stein also observed a change in the slope of the Hoffman–Weeks plot occurring at about 160°C with the value for T_m° obtained from crystallization temperatures above 160°C being about 25°C higher than that obtained from crystallization data below 160°C. The T_m° obtained from the high T_c data was taken as being more representative of the true value of T_m° for PVF_2. The change in slope was attributed to fewer of the head-to-head linkages being trapped in the crystals at higher crystallization temperatures. A change in the slope of the Hoffman–Weeks plot was also observed in this work but it occurred at a lower temperature (about 150°C for the pure PVF_2 and at progressively lower temperatures for the decreasing PVF_2 content blends). All data shown in *Figure 2* (and hence all T_m° values) is for crystallization temperatures above the observed change in slope. The PVF_2 examined in this work was from a different manufacturer than that studied by Morra and Stein and has a lower molecular weight and may contain significantly more head-to-head linkages which would account for the observed differences in T_m° for two PVF_2 resins from different manufacturers.

The extrapolated melting points of the 60/40 and 80/20 blends are below those of the 50/50 blend although they should be equivalent. At equilibrium, the intersection of the binodal (cloud point curve) and the melting point curve should be a horizontal line with all compositions containing greater than 50% PVF_2 having the same T_m° (see for example T_2 in *Figure 1*). The reason for the discrepancy between the expected and observed T_m°'s is probably due to the system not reaching equilibrium during crystallization. Below the melting point the system should consist of a uniform population of crystals in equilibrium with an amorphous phase containing PEA and a small amount of PVF_2. The system probably never reaches this state because prior to crystallization the melt has undergone phase separation and contains PVF_2 rich domains in a PVF_2 poor matrix (or the converse), and upon lowering the temperature below T_m° the system does not redistribute to the equilibrium compositions corresponding to T_c before crystallization occurs. Because the local composition (and probably the morphology) in the crystallized PVF_2 rich domains is different from that in the matrix, the crystals in the different regions will melt at different temperatures giving rise to difficulties in measuring T_m°. Hence the variation of the equilibrium melting points of the 60/40 and 80/20 blends is probably due to morphological factors influencing the accuracy of the measurement of T_m°.

The values of T_m° and the cloud points in *Table 1* are plotted to give the α-PVF_2/PEA phase diagram shown in *Figure 3*. The cloud point curve and equilibrium melting point curve intersect at about 180°C and a composition of 50% by weight PVF_2. The cloud point curve can be measured at temperatures less than the melting point in the region of 50% PVF_2 (the portion of cloud point curve given by a broken line in *Figure 3*) because just below the equilibrium melting point the rate of crystallization is very slow compared to the rate of phase separation.

As mentioned previously there was no observable one phase region in the melt at compositions greater than 55% PVF_2 leading to the conclusion that the phase separation curve is highly skewed towards the PVF_2 rich side of the phase diagram. This type of skewness is opposite to what one would predict on the basis of the molecular weight differences between the PVF_2 and the PEA using a theory based on the Flory–Huggins formulation for the combinational entropy. This has also been observed in the cloud point curves of PVF_2 with isotactic poly(ethyl methacrylate)[7,15]. On further examination the measured cloud point curve appears to be shaped slightly concave downwards suggesting an 'hourglass' type phase separation curve[17]. If one combines a skewed hourglass type of phase diagram with one side very close to the pure B component side of the phase diagram (as shown in *Figure 4a*) with the melting point curve (shown in *Figure 4b*) the resulting phase diagram (*Figure 4c*) closely matches the observed α-PVF_2/PEA phase diagram in character. Whether the system actually has an 'hourglass' shaped binodal or true *LCST* behaviour below T_m° is not really significant because, strictly speaking, the binodal cannot be defined below the melting point curve.

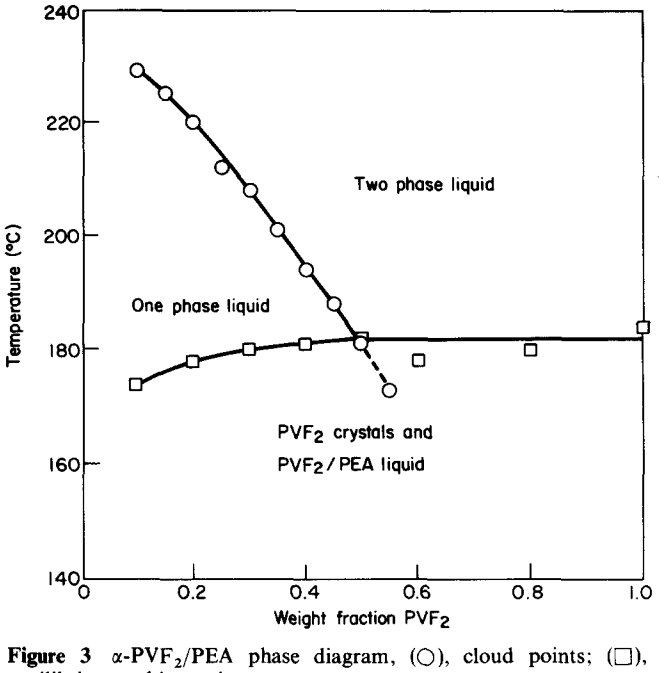

Figure 3 α-PVF_2/PEA phase diagram, (○), cloud points; (□), equilibrium melting points

The phase diagram shown in *Figure 3* agrees with the phase diagram presented by Endres *et al.*[10] except that Endres *et al.* also give data indicating the position of the binodal at concentrations greater than 60% PVF_2. They measured the PVF_2 rich side of the phase diagram indirectly by d.s.c. experiments. If this portion of the binodal is valid it should be possible to measure the corresponding cloud points, yet in the turbidity experiments reported by Endres *et al.* and in our work it was not possible to measure cloud points in this region of the phase diagram.

The melting point depression observed for the α-PVF_2 at compositions of 50% PVF_2 and less (where crystallization is occurring from a homogeneous melt) can be used to estimate the polymer–polymer interaction parameter, χ, following the treatment of Nishi and Wang[5]. The melting point depression of the crystalline polymer blended with an amorphous polymer in a compatible blend can be written as

$$\left(\frac{1}{T_{mB}^\circ}-\frac{1}{T_m^\circ}\right)=\frac{-Rv_2}{v_1\Delta H_2}\left[\frac{\ln\phi_2}{m_2}+\left(\frac{1}{m_2}-\frac{1}{m_1}\right)(1-\phi_2)+\chi(1-\phi_2)^2\right] \quad (1)$$

where T_{mB}° and T_m are the equilibrium melting points of the blend and homopolymer respectively, ΔH_2 is the heat of fusion for the 100% crystalline homopolymer, v_1, v_2 are the molar volumes of the repeat units of the noncrystallizable and crystallizable components respectively, and ϕ_1, ϕ_2 are the volume fractions of the noncrystallizable and crystallizable polymers. If both components are high molecular weight polymers (m_1, $m_2 \gg 1$) then equation (1) reduces to

$$\left(\frac{1}{T_{mB}^\circ}-\frac{1}{T_m^\circ}\right)=\frac{-Rv_2}{v_1\Delta H_2}[\chi(1-\phi_2)^2] \quad (2)$$

If we ignore entropic contributions to χ then we can write[17]:

$$\chi=\frac{Bv_1}{RT} \quad (3)$$

where B is the interaction energy density. Combining

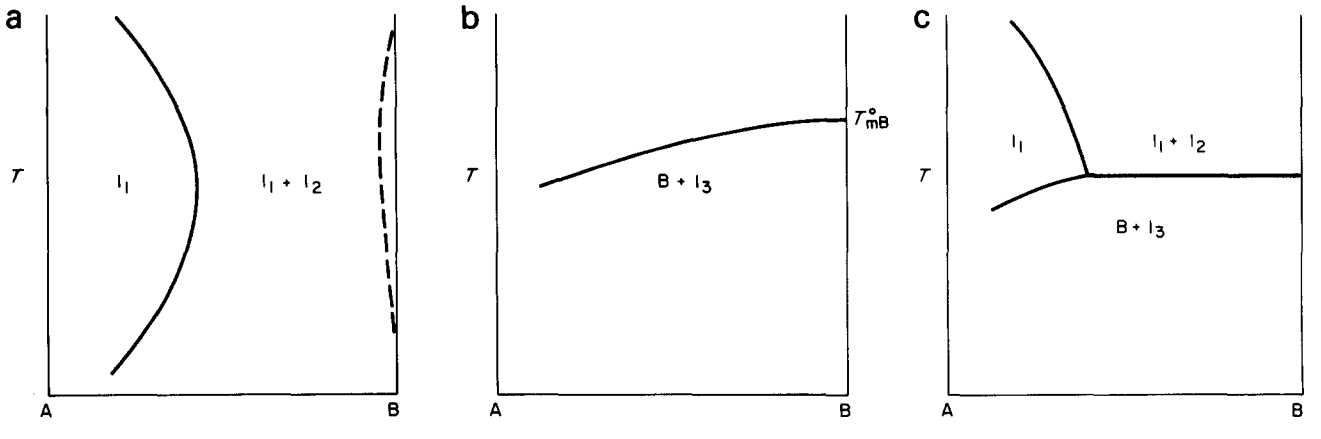

Figure 4 (a) Highly skewed 'hourglass' type phase diagram; (b) melting point curve; (c) schematic phase diagram resulting from the overlap of (a) and (b), note the similarity to *Figure 3*

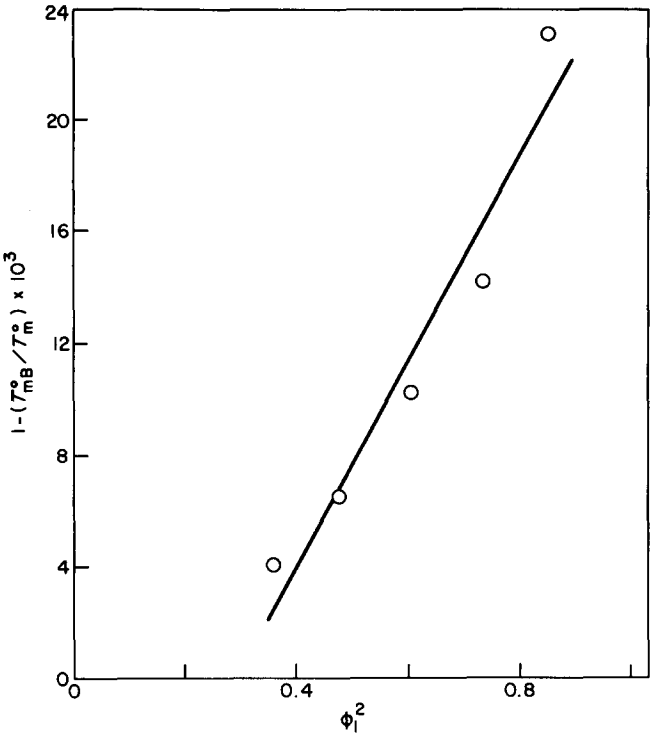

Figure 5 Plot of $(1-T^\circ_{mB}/T^\circ_m)$ *versus* ϕ_1^2 used to obtain χ

equations (2) and (3) yields

$$\left(\frac{1}{T^\circ_{mB}}-\frac{1}{T^\circ_m}\right)=\frac{-Rv_2}{v_1\Delta H_2}\left(\frac{v_1 B}{RT}\right)\phi_1^2 \tag{4}$$

upon rearranging with $T=T^\circ_{mB}$

$$(1-T^\circ_{mB}/T^\circ_m)=\frac{-Bv_2}{\Delta H_2}(\phi_1)^2 \tag{5}$$

and a plot of $(1-T^\circ_{mB}/T^\circ_m)$ *versus* ϕ_1^2 should give a straight line of slop $-Bv_2/\Delta H_2$. *Figure 5* shows such a plot and from the least squares line a value of $B=-1.59\,\text{cal/cm}^3$ is obtained using the constants $\Delta H_2=1600\,\text{cal/mol}$[18] and $v_2=36.4\,\text{cm}^3/\text{mol}$.[11] This corresponds to a value of $\chi=-0.16$ at 170°C (assuming $v_1=90.2\,\text{cm}^3/\text{mol}$[7]).

Figure 6 is a plot of the spherulite growth rates for various composition blends as a function of crystallization temperature. In all cases it was only possible to measure the high temperature portion of the growth rate curve (where the negative temperature dependence of G is controlled mainly by the nucleation rate) due to the high nucleation density present at low crystallization temperatures (which prevented measurements below about 130°C). If the growth rates in *Figure 6* are plotted *versus* undercooling instead of against T_c the curves are shifted closer together due to the change in equilibrium melting point with composition.

The spherulite growth rate curves can be analysed following the treatment of Hoffman, Davis and Lauritzen[19] using a growth rate expression involving the product of two exponentials with an added concentration dependent term[20,21] (equation (6))

$$G=G_0C^\alpha\exp\left(\frac{-U^*}{R(T_c-T_\infty)}\right)\exp\left(\frac{-K_g}{T_c\Delta Tf}\right) \tag{6}$$

where G_0 is a pre-exponential factor, C is the concentration of crystallizable polymer, α is the power law exponent for the concentration dependence of the growth rate, U^* is the jump rate energy, T_∞ is the temperature at which segmental motion stops (usually taken at $T_g-30\,\text{K}$), K_g is the nucleation factor containing the surface free energies, equilibrium melting point and heat of fusion, ΔT is the undercooling and f is the correction factor for the heat of fusion [necessary at large supercoolings; $f=2T_c/(T^\circ_m+T_c)$]. The normal procedure for determining K_g and G_0 involves plotting $\ln G+U^*/R(T_c-T_\infty)$ *versus* $1/T_c\Delta Tf$ with the values of U^* chosen so as to give the best fit least squares line through the data. Because the data collected for the PVF_2/PEA blends includes only the nucleation controlled portion of the curve, the choice of a value for U^* becomes somewhat arbitrary. In addition, U^* may depend on composition in an unknown manner. Trying values of U^* over a wide range (1000–10 000 cal/mol) had essentially no effect on the fit of the data to equation (6). To simplify the analysis, and to avoid any *ad hoc* assumptions about the nature of U^*, the jump rate term (which is not changing significantly over the range of crystallization temperatures studied) can be combined with the preexponential factor. The concentration dependence can also be included in the preexponential factor (assuming α to be temperature independent). The resulting simplified equation is

$$G=G_1\exp\left(\frac{-K_g}{T_c\Delta Tf}\right) \tag{7}$$

A plot of $\ln G$ *versus* $(1/T_c\Delta Tf)$ should give a straight line with a slope of $-K_g$ and an intercept of $\ln G_1$. *Figure 7* shows typical plots for the homopolymer and the 30/70 composition blend and the corresponding least squares fit

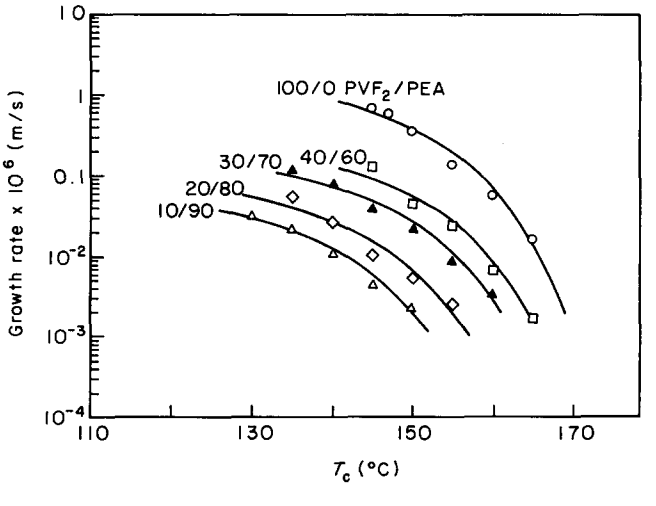

Figure 6 Spherulite growth rates *versus* crystallization temperature for the various blend compositions

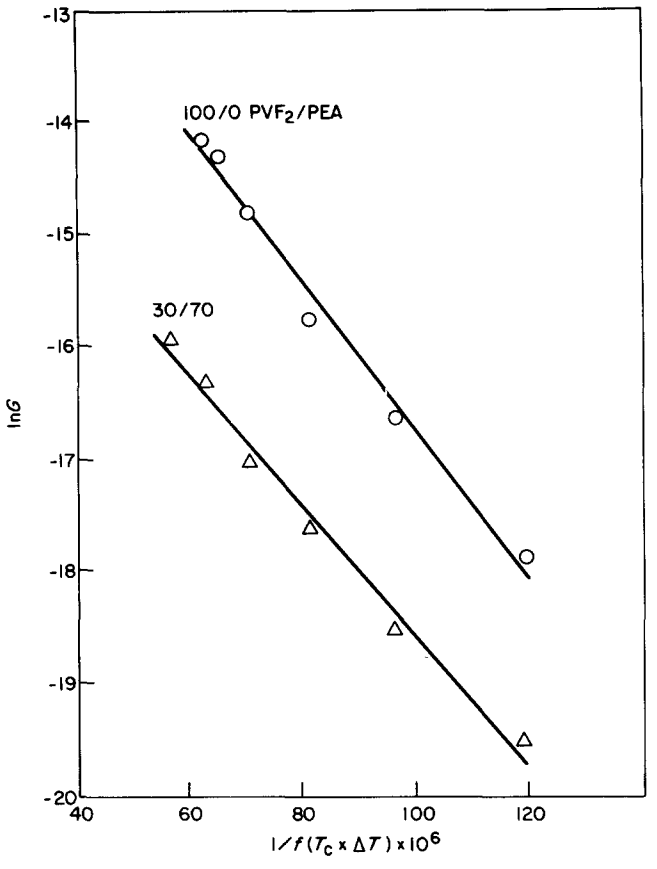

Figure 7 Typical plots of ln$G$ *versus* $1/fT_c\Delta T$ for pure PVF_2 and the 30/70 PVF_2/PEA blends

lines. The values for K_g and G_1 are given in *Table 2*. G_1 shows a slight dependence on composition, which is to be expected since G_1 contains the C^α term (α has usually been found to be less than one for polyethylene in low molecular weight solvents[20,21]) and the $\exp(-U^*/R(T_c-T_\infty))$ term where U^* may be composition dependent. Unlike the blend system PVF_2/PMMA which has been studied by other authors[11,22], the glass transition in the present system does not depend strongly on composition. The T_g of PVF_2 is -30 to $-50°C$[9], the T_g of PEA is $-25°C$[23], hence T_∞ can be taken as approximately constant. Nevertheless, the transport properties of the two polymers at the crystallization temperature are not equivalent and U^* might be expected to vary with composition. The usual procedure of plotting ln G *versus* ln C to obtain α would be complicated by a dependence of U^* on concentration (which is not a problem in dilute solution crystallization[20,21]) and would preclude this type of analysis. The values of K_g obtained from the analysis vary somewhat with composition but no discernible trend is evident. The average value of K_g is $61\,700\,K^2$.

The Lauritzen Z test is generally used to give an indication of whether crystallization is occurring in regime I or II[19,24]. Z is given by

$$Z \simeq 10^3(L/2a_0)^2 \exp\left[\frac{-X}{T_c\Delta T}\right] \qquad (8)$$

where L is the substrate length, and a_0 is the fold width parallel to the growth face. With X set to K_g and $Z \leqslant 0.01$ the crystallization is occurring in regime I. For $X = 2K_g$ and $Z \geqslant 1$ regime II is valid. According to Hoffman *et al.*[19] the calculated value of K_g is generally inserted into equation (8) and the regime which yields a realistic value for L is taken as being correct. For $K_g = 61\,700\,K^2$ and $a_0 = 0.441$ nm (spacing of the (110) planes for α-PVF_2[9,13]) an assumption of regime I leads to values of L never exceeding about 0.2–0.3 nm over the entire composition and temperature range examined. If regime II is assumed L varies from a few nanometers to tens of nanometers over the same composition and temperature range. Clearly the Z test points to regime II crystallization (which has been observed with PVF_2/PMMA blends over a similar range of crystallization temperatures by Wang and Nishi[22]).

Regime II crystallization leads to the following equation for K_g[20]

$$K_g \text{ (regime II)} = 2b_0(\sigma\sigma_e)T_m^\circ/\Delta H_f k$$

where b_0 is the thickness of a fold perpendicular to the growth face (the (110) interplanar spacing in the crystal[9,13]), ΔH_f is the heat of fusion of pure PVF_2 and $\sigma\sigma_e$ is the product of the surface free energies of the crystal. With $b_0 = 0.441$ nm and $\Delta H_f = 1.87 \times 10^8$ J/m^3 the corresponding value of $\sigma\sigma_e$ is 4.4×10^{-4} J^2/m^4 (440 erg^2 cm^{-4}) for α-PVF_2 crystals. This is close to the values obtained by Wang and Nishi previously for PVF_2/PMMA blends[22].

As the concentration of PEA is increased the texture of spherulites grown from the melt becomes more open. *Figure 8* is a series of optical micrographs with phase contrast optics, and crossed polarizer and analyser, of spherulites grown at a crystallization temperature of 150°C showing the progressive change in the texture from pure PVF_2 (*Figures 8a,b*) to the 15/85 concentration blend (*Figures 8i,j*). The radiating branches of the spherulites become more distinct as the PVF_2 content decreases. In the pure PVF_2 spherulites a radiating texture can be observed but individual branches (bundles of lamellae) cannot be distinguished. In the 45/55 PVF_2/PEA and lower PVF_2 content blends the branching texture of the spherulites can be observed clearly. Rejection and segregation of the noncrystallizable PEA to the channels between the branches of the spherulites is occurring as the molten blend surrounding the growing lamellae is depleted of PVF_2 during crystallization. The spherulites in the 45/55 and lower PVF_2 content blends (*Figures 8c–j*), while essentially volume (area) filling, never completely impinge indicating that as the growth fronts of two spherulites approach each other the intervening region becomes depleted of PVF_2

Table 2 G_1 and K_g values for PVF_2/PEA blends of various compositions

PVF_2/PEA Concentration (by weight)	G_1 (m s^{-1})	K_g (K^2)
100/0	4.32×10^{-5}	66600
40/60	2.92×10^{-6}	51300
30/70	3.00×10^{-6}	58300
20/80	2.42×10^{-6}	67600
10/90	1.52×10^{-6}	65000

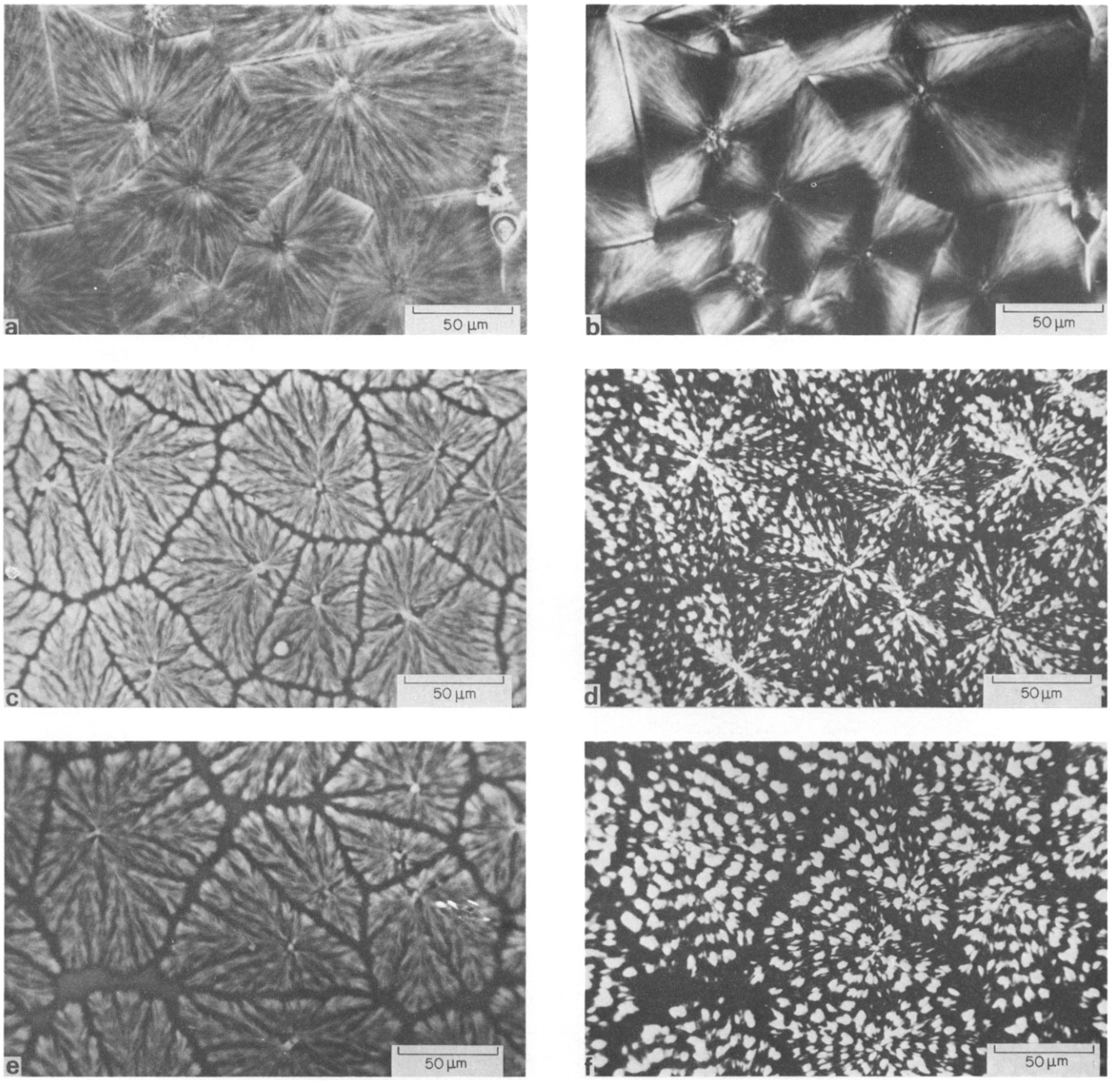

Figure 8 Optical micrographs (phase contrast optics, and crossed polarizer and analyser) of spherulites grown at $T_c = 150°C$ for the various blends; (a,b) 100/0 PVF_2/PEA; (c,d) 45/55; (e,f) 35/65; (g,h) 25/75; (i,j) 15/85. All micrographs are the same magnification

thereby halting crystallization before impingement. The spacing of the extinction rings (due to lamellar twist) in the spherulites observed in polarized light changes pronouncedly with PEA content. *Figure 9* is a plot of the ring spacing versus crystallization temperature for pure α-PVF_2 and the various blend compositions. The ring periodicity depends on both crystallization temperature and blend composition. As is usually the case in polymer spherulites the ring periodicity (seen most clearly in *Figures 8f,h*) becomes larger with increasing T_c as has been observed in α-PVF_2 in the past[25]. In addition, the ring spacing increases with increasing PEA content at constant T_c. This dependence of band periodicity on diluent content has been previously observed in PVF_2/PMMA blends[26] and polyethylene/paraffin blends[27].

The implications of the composition dependence of the spherulite ring periodicity concerning the role of cooperative effects between twisted lamellae, as well as the details of the evolution and fine structure of the spherulites and the nature of the underlining crystal habits of their constituent lamellae, will be discussed in a future paper[28].

CONCLUSIONS

The phase diagram for the α-PVF_2/PEA blend system has been established. The blend exhibits overlapping phase separation and crystallization behaviour with the intersection of the cloud point curve (binodal) and the melting point curve occurring at about 180°C and a composition of 50/50 PVF_2/PEA by weight. At temperatures above the cloud point the system phase

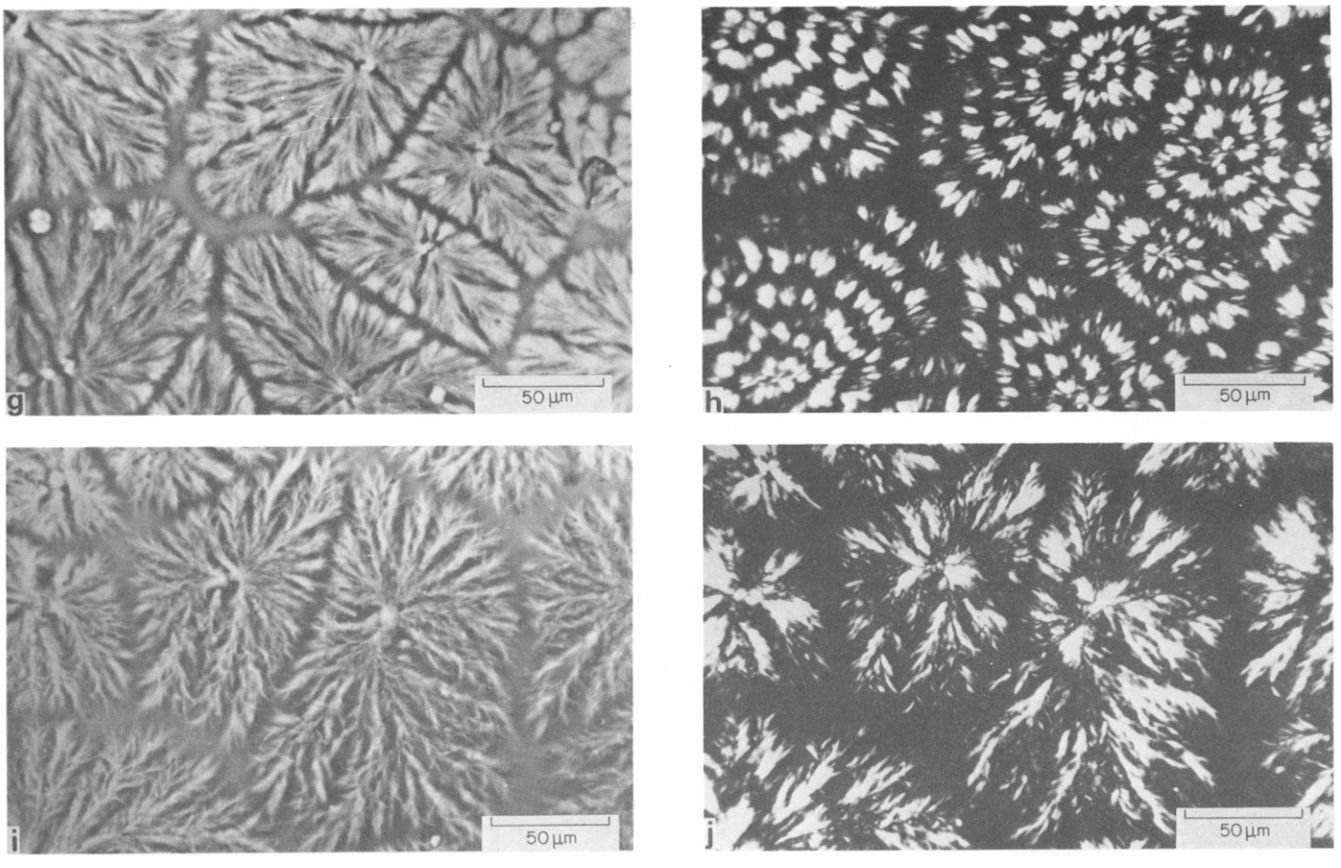

Figure 8 continued

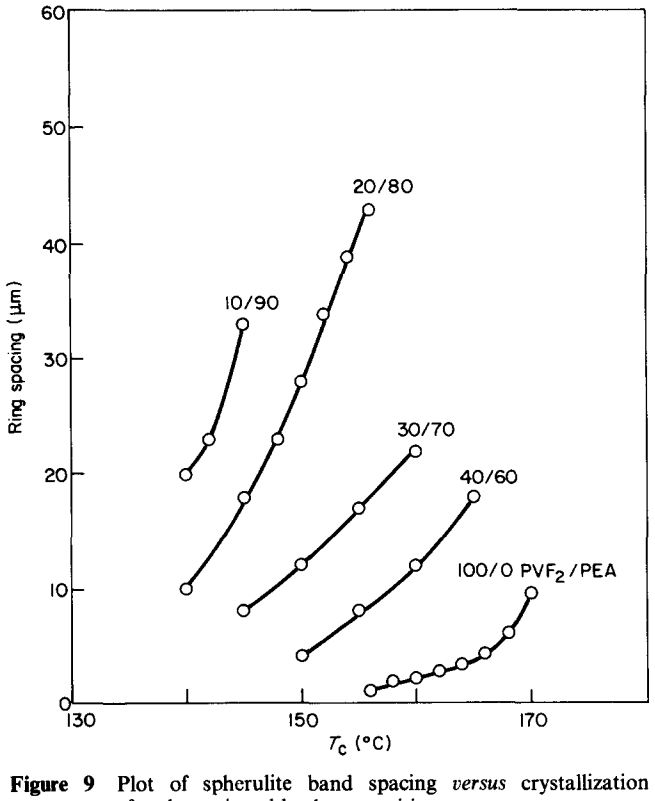

Figure 9 Plot of spherulite band spacing *versus* crystallization temperature for the various blend compositions

separates into two liquid phases indicative of *LCST* behaviour. The cloud point curve is highly skewed towards the PVF_2 rich side of the phase diagram with the half of the cloud point curve closest to the PVF_2 axis occurring at greater than 95/5 PVF_2/PEA concentrations (the highest content PVF_2 sample examined).

From the melting point depression of the PVF_2 (at less than 55% PVF_2 concentrations) a value of the interaction density $B = -1.59\,\text{cal}\,\text{g}^{-3}$, was obtained. The corresponding polymer–polymer interaction parameter is $\chi = -0.16$ (at 170°C). The negative value of χ is consistent with the observed compatibility of the polymers in this composition range.

Isothermal spherulite growth rates (upon cooling from the one phase melt) measured as a function of temperature and PVF_2 content show a slight dependence on composition (when the actual undercooling is considered). This dependence is probably due to a combination of changes in the jump rate energy, U^*, for segmental motion and a dependence of the growth rate on concentration. The Lauritzen Z test indicates that crystallization probably occurs in regime II. The value of the product of the surface free energies $\sigma\sigma_e$ calculated from the growth rate curves is $4.4 \times 10^{-4}\,\text{J}^2\,\text{m}^{-4}$.

The texture of the α-PVF_2 spherulites becomes more open with increasing PEA content and the periodicity of the extinction rings (observed in polarized light) becomes larger with increasing T_c, and with increasing PEA content at constant T_c.

ACKNOWLEDGEMENTS

The research presented in this paper was conducted while one of the authors (RMB) held a National Research Council Postdoctoral Research Associateship. Discussions with Dr G. T. Davis are gratefully acknowledged.

REFERENCES

1 Olabisi, O., Robeson, L. M. and Shaw, M. T. 'Polymer–Polymer Miscibility', Academic Press, 1979, Ch. 7
2 Krause, S. 'Polymer Blends', Vol. 1, (Ed. D. R. Paul), Academic Press, New York, 1978, Ch. 2
3 Bernstein, R. E., Paul, D. R. and Barlow, J. W. *Polym. Eng. Sci.* 1978, **18**, 683
4 Noland, J. S., Hsu, N. N. C., Saxon, R. and Schmitt, J. M. *ACS Adv. Chem.* 1971, **99**, 15
5 Nishi, T. and Wang, T. T. *Macromolecules* 1975, **8**, 909
6 Roerdink, E. and Challa, G. *Polymer* 1980, **21**, 1161
7 Paul, D. R., Barlow, J. W., Bernstein, R. E. and Wahrmund, D. C. *Polym. Eng. Sci.* 1978, **18**, 1225
8 Wahrmund, D. C., Bernstein, R. E., Barlow, J. W. and Paul, D. R. *Polym. Eng. Sci.* 1978, **18**, 677
9 Lovinger, A. J. 'Developments in Crystalline Polymers', (Ed. D. C. Bassett), Applied Science Publishers, New Jersey, 1982, Ch. 5
10 Endres, B., Garbella, R. W. and Wendorff, J. H. *Colloid Polym. Sci.* 1985, **263**, 361
11 Morra, B. S. and Stein, R. S. *J. Polym. Sci., Polym. Phys. Edn.* 1982, **20**, 224
12 Certain equipment, instruments or materials are identified with trade names in this paper in order to adequately specify the experimental details. Such identification does not imply recommendation or endorsement by the National Bureau of Standards, nor does it imply the materials or equipment identified are necessarily the best available for the purpose
13 Briber, R. M. and Khoury, F. *ACS Polym. Prepr.* 1985, **26(2)**, 310
14 Hoffman, J. D. and Weeks, J. J. *J. Res. Natl. Bur. Stand.* 1962, **66**, 13
15 ten Brinke, G., Eshuis, A., Roerdink, E. and Challa, G. *Macromolecules* 1981, **14**, 867
16 Sanchez, I. C. 'Polymer Blends', Vol. 1, (Ed. D. R. Paul), Academic Press, New York, 1978, Ch. 3
17 Scott, R. L. *J. Chem. Phys.* 1949, **17**, 279
18 Nakagawa, K. and Ishida, Y. *J. Polym. Sci., Polym. Phys. Edn.* 1973, **11**, 2153
19 Hoffman, J. D., Davis, G. T. and Lauritzen, J. I. 'Treatise on Solid State Chemistry', Vol. 3, (Ed. N. B. Hannay), Plenum Press, New York, 1976, Ch. 3
20 Keller, A. and Pedemonte, E. *J. Cryst. Growth* 1973, **18**, 111
21 Cooper, M. and Manley, R. St. J. *Macromolecules* 1975, **8**, 219
22 Wang, T. T. and Nishi, T. *Macromolecules* 1977, **10**, 421
23 Brandup, J. and Immergut, E. H. 'Polymer Handbook', John Wiley, New York (1975)
24 Lauritzen, Jr., J. I. *J. Appl. Phys.* 1973, **44**, 4353
25 Lovinger, A. J. *J. Polym. Sci., Polym. Phys. Edn.* 1980, **18**, 793
26 Morra, B. D. and Stein, R. S. *Polym. Eng. Sci.* 1984, **24**, 311
27 Keith, H. D. and Padden, Jr., F. J., private communication
28 Briber, R. M. and Khoury, F., in preparation